ORIGINAL ARTICLE

Asymmetry in the spin-up of a stratified fluid in a sliced, square cylinder

R. J. Munro[1] · M. R. Foster[2,3]

Abstract

Previously, we have reported theory and experiments on the spin-up of a linearly strati-fied fluid contained in a sealed square cylinder with a bottom sloped at angle α (Munro & Foster, *Phys. Fluids*, **26**, 026603, 2014). The motion is characterized by the small Rossby number, ϵ, the fractional change in the rotation rate, the Ekman number, E, and the Burger number, S, the square of the ratio of the buoyancy frequency (or Brunt-Väisälä frequency) to the base rotation rate. This paper, supplementing what has gone before, is focused on the horizontal and vertical structure of the propagating vorticity waves (Rossby waves), with alternating anti-cyclonic and cyclonic cells, which move across the tank from east to west, thereby accomplishing at least the early stages of the spin-up. We find strong dependence of the modal structure of these Rossby waves, and their speed, on the Burger number. How-ever, what is particularly noteworthy is the observed strong north-south asymmetry of the wave field. We find that the asymmetry is not consistent with typical Rossby-wave theories (Pedlosky and Greenspan, *J. Fluid Mech.*, **27**, p. 291, 1967), but is attributable to second-order effects in the asymptotic expansion of the streamfuntion in powers of α.

Keywords Stratified · Rotating flow · Rossby waves

1 Introduction

The classic problem of spin-up has been studied extensively, using homogeneous [1–3] and stratified [4–6] fluids. A typical spin-up problem is concerned with how a contained fluid adjusts from one state of solid rotation to another, due to an increase in the rotation rate of the containing vessel. Previous studies have focussed mostly on axisymmetric spin-up

✉ R. J. Munro
  rick.munro@nottingham.ac.uk

  M. R. Foster
  foster.9@osu.edu

1 Faculty of Engineering, University of Nottingham, Nottingham NG7 2RD, UK

2 Department of Mechanical Engineering, Western New England University, Springfield, MA 01119, USA

3 Department of Mechanical and Aerospace Engineering, The Ohio State University, Columbus, OH 43210, USA

of a uniform density (or homogeneous) fluid in a circular cylinder, in the linear regime, *i.e.* the Rossby number, $\epsilon = \Delta\Omega/\Omega$, is small. Here, $\Omega - \Delta\Omega$ and Ω denote the initial and final rotation rates, respectively. Under these conditions the resulting flow is axisymmetric, with the fluid spun up on the time scale $E^{-1/2}\Omega^{-1}$ by the secondary, meridional flow that develops in fluid's interior, driven by radial transport through the Ekman boundary layers at the tank's base and lid (if present), which is returned to the interior via the vertical shear layers (or Stewartson layers) that form on the container's sidewall [7]. Here, $E = \nu/\Omega L^2$ is the Ekman number, where L is a characteristic length scale. Within the interior, the secondary circulation acts to stretch the background vortex and draw fluid radially inwards, which by conservation of angular momentum must acquire greater angular velocity.

The effect of a stable, continuous density stratification on the spin-up process was studied by Walin [5]. In this case, the density stratification inhibits the formation of Stewartson layers and hence the meridional circulation–as a result, the radial Ekman transport, on reaching the sidewall, erupts into the inviscid interior. As a consequence, the spin-up process is only able to penetrate to a height (or depth) of order $S^{-1/2}L$, where $S = (N/\Omega)^2$ and N are the Burger number and buoyancy frequency, respectively. As a result, the limiting state on the spin-up time scale, $E^{-1/2}\Omega^{-1}$, is a spatially non-uniform rotation—the final near-spun-up state is approached only on the much longer viscous timescale, $E^{-1}\Omega^{-1}$. The review articles by Benton & Clark [8] and Duck & Foster [9] provide a general overview of homogeneous and stratified spin-up.

More recently, following initial work by van Heijst [10], spin-up has been studied in a variety of non-axisymmetric containers, including rectangular, square and semicircular cylinders [10–16], for small and moderate Rossby number, and for the limiting case of spin-up from rest, *i.e.* $\epsilon = 1$. In all of these studies, the initial starting flow, when observed in the co-rotating reference frame, is a two-dimensional anticyclonic flow with closed streamlines that completely fill the container's interior. However, when the Rossby number is not small, intense cyclonic vortices quickly form in the vertical-corner regions of the container, due to the unsteady separation of the sidewall boundary layers, a mechanism studied in detail by Munro *et al.* [15] for the case of a square cylinder with $\epsilon = 1$. These cyclonic vortices grow rapidly and deform the initial anticyclonic cell. In the square cylinder, due to its $\pi/2$ rotational symmetry, the secondary vortices form symmetrically and so remain confined to the corner regions, with the deformed initial anticyclone throughout occupying the central region of the tank. In contrast, in a rectangular container, large cyclonic vortices form downstream of the two long sides, which rapidly grow to a size comparable with the container's width, leading to the formation of a stable array of alternate anticyclonic and cyclonic cells of equal size, with the number of cells determined by the container's aspect ratio [11]. Similarly, in a semicircular cylinder, we observe the eventual formation of an array of three alternate cells [10, 16].

Non-axisymmetric spin-up has also been studied in containers with an inclined base. Of particular importance is the study by Pedlosky & Greenspan [17] of linear spin-up of a homogeneous fluid in a sliced circular cylinder (*i.e.* a closed cylinder with its base plane inclined at an angle α to the horizontal). The variation in depth in the sliced cylinder, when rotating, induces motions like those arising due to the Coriolis parameter variation with latitude on a rotating sphere (*i.e.* the β effect). Indeed, the primary motivation for the work by Pedlosky & Greenspan [17], and subsequent related studies [18, 19], was to gain a better understanding of the ocean circulation at mid-latitudes over scales large enough to require inclusion of the β effect. The presence of the base slope gives rise to two-dimensional vorticity waves (*i.e.* Rossby waves) which form with alternating sense circulation, and propagate "westwards" across the slope gradually filling the fluid's interior. For

$E^{1/2} \ll \alpha$ (the most physically relevant case—indicating the Ekman layer thickness is small in comparison to the vertical extent of the slope), the Rossby waves are the dominant spin-up mechanism. More recently, Munro & Foster [20, 21] extended consideration to spin-up of a linearly stratified fluid in sliced square and circular cylinders. They showed that the background density gradient can significantly affect the structure and characteristics of the vorticity waves produced. In particular, when the Burger number S is not small, the vorticity waves are confined to a region of height $S^{-1/2}L$ above the mean slope elevation, and that both the propagation speed and decay rate of the waves increase with S.

This paper provides significant additions to what has been reported in our previous paper [20]. There, we compared the theory developed in that paper with a set of experiments; principally, those comparisons were of velocity profiles across the mid-height of the tank, at particular times. The theory/experiment agreement is quite good, but those results are not reiterated here. By contrast, here we report instantaneous streamline maps, which show the vorticity waves (Rossby waves) propagating from "east" to "west" across the tank. We also show those streamline patterns at differing vertical locations in the container, in order to elucidate the S-related depth-dependence of the motion–in particular, the "trapping" of much of the Rossby-wave induced spin-up near the bottom of the tank. Of the significant new results reported in Sect.2.3, we briefly note three here. First, we find that the wave structure is quite complicated at $S = 0$, with many length scales in evidence, but at strong stratification, for S larger than, say, 1, only the first few modes are observed, moving across the tank. That observation is consistent with the theoretical results previously reported that the Rossby-wave damping increases with increasing values of S [20]. Secondly, we note that the speed of the waves also increases with increasing S. Finally, in all of the Rossby-wave analyses in the literature of which we are aware (see, for example, [18, 19, 22] and [20]),the waves exhibit north-south symmetry. However, experimental results in Figs. 2, 3, 4, 5, 6 show significant north-south asymmetry, and all the more as S increases. In Sect.3, we show that the first term in an asymptotic series for the streamfunction in powers of the slope α does indeed have north-south symmetry, evident in Fig. 7. However, we determine that second term in that series exhibits asymmetry. Since for us $\alpha = 0.175$ ($= 10°$), we expect that the inclusion of this second term in the series will alter the symmetry in Fig. 7 significantly. Development of that higher-order theory is not reported here. Finally, there are many facets of the observations—for example the boundary-layer-induced vortex formation, not solely confined to the corners—that need further in-depth analysis, but we leave that for another time.

2 Experiments

2.1 Apparatus and set-up

The experiments were performed in a transparent acrylic tank with a square plan-view section of width $L = 35$ cm and base plane inclined at angle $\alpha = 10°$ (0.175 rad) to the horizontal. The tank was mounted on a variable-speed turntable, with the tank's central, vertical axis coincident with the axis of rotation. A sketch of the experimental set-up is shown in Fig. 1. With the turntable stationary, the tank was filled either with a homogeneous salt-water solution (density $\rho_0 = 1.03$ g/cm^3), or a linearly stratified salt-water solution with buoyancy frequency $N = [g(\rho_b - \rho_t)/\rho_t H]^{1/2}$. Here, ρ_t and ρ_b denote the liquid density at the free surface and at the centre of the base plane, respectively. The salt used was NaCl. The linear density
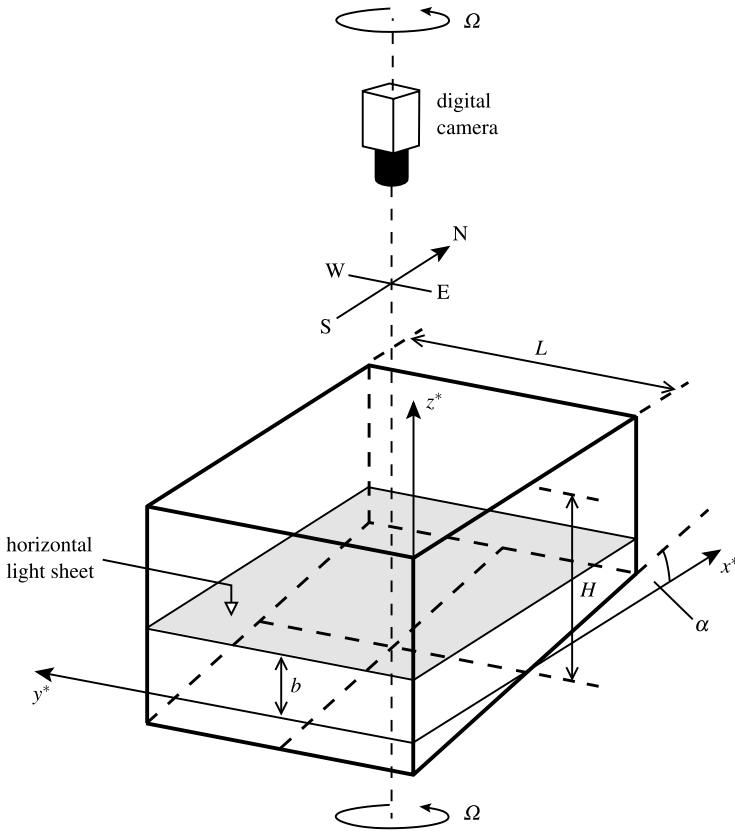
Fig. 1 A sketch of the experimental set-up

gradient was produced and measured using the standard techniques described in Economidou & Hunt [23]. Once filled, the tank was sealed with a rigid transparent lid, designed to completely displace the liquid's surface, to prevent the entrapment of air pockets on the lid's underside. Here, H denotes the mean depth of the sealed liquid, *i.e.* the depth along the tank's central, vertical axis, between the centre of the base slope and the underside of the lid. In all cases, $H = 23$ cm.

With the initial set-up complete, the turntable was carefully brought from rest into anticlockwise rotation and its angular frequency gradually increased to its initial value $\Omega - \Delta\Omega$. The apparatus were then left rotating at the initial rate to allow the liquid to reach a state of near-solid-body rotation. Once in this state, the experiment was initiated (at time $t^* = 0$) by increasing the angular frequency to its final value, Ω.

The key dimensionless parameters for this problem are the Burger (S), Ekman (E) and Rossby (ϵ) numbers, defined here as

$$S = (N/\Omega)^2, \ E = \nu/\Omega L^2, \ \epsilon = \Delta\Omega/\Omega \qquad (1a\text{–}c)$$

where ν denotes kinematic viscosity. In all experiments the aspect ratio $h = H/L \approx 0.66$ was fixed. Table 1 shows the key parameters for the experiments reported here. In all cases, $E = \mathcal{O}(10^{-5})$ or less, with the Rossby number throughout fixed at $\epsilon = 0.02$. Under these

Table 1 The key parameters for each experiment: S, E and ϵ are defined in Eq. (1). Also shown are values of the dimensionless vertical length scale, $S^{-1/2}$

Label	Ω (rad/s)	S	$E\,(10^{-5})$	ϵ	$S^{-1/2}$
A	1.1	0.0	0.74	0.02	
B	1.04	0.5	0.78	0.02	1.4
C	1.04	1.1	0.78	0.02	0.95
D	0.48	5.0	1.7	0.02	0.45
E	0.34	10	2.4	0.02	0.32
F	0.24	20	3.4	0.02	0.22

conditions, it is the Burger number that affects the formation and structure of the stratified Rossby waves, which here was varied between $S = 0$ and 20. The Schmidt number for NaCl in water is approximately 670 [24] and so effects associated with salinity diffusion are henceforth considered negligible.

2.2 Measurements and notation

Measurements of fluid velocity were obtained using two-dimensional PIV. Small, seeding particles were suspended within the water column during the initial set-up, and illuminated by a thin horizontal light sheet positioned at a height b above the centre of the base plane (see Fig. 1). For the homogeneous case, the density of the salt-water solution (ρ_0) was matched to the mean density of the particles (1.03 g/cm^3), and the water column well stirred to evenly distribute the particles. For the stratified case, the particles were carefully added and allowed to settle freely into suspension in a narrow horizontal band about their mean-density level, with the densities ρ_t and ρ_b chosen to achieve the desired buoyancy frequency, N, while ensuring the water density at height b above the centre of the base plane corresponded to the mean particle density.

For times $t^* \geqslant 0$, the in-plane particle motion was recorded using a digital video camera positioned above the tank (see Fig. 1). Both the lighting unit and camera were mounted on the turntable to allow the images to be recorded in the co-rotating reference frame. The images were recorded at 10 Hz, with 1280×1024 pixel resolution. PIV calculations were performed using square interrogation windows (13×13 pixels), overlapped to achieve 10-pixel spacing between velocity vectors. The corresponding spacing between the measured velocity vectors was at most 0.4 cm. In all experiments, images were captured for a duration of 16 min, which in all cases was comparable to the standard spin-up time scale, $E^{-1/2}\Omega^{-1}$.

The velocity data were calculated and analysed relative to the rotating reference frame, (x^*, y^*, z^*), which is shown in Fig. 1. The corresponding velocity components are denoted $\mathbf{u}^* = (u^*, v^*, w^*)$. Here, x^* and y^* denote the up-slope and along-slope directions, respectively, and z^* denotes vertical height, with the horizontal plane $z^* = 0$ passing through the centre of the inclined base plane (see Fig. 1). Hence, the rotation axis is located at $(x^*, y^*) = (L/2, L/2)$, and the inclined base plane defined by $z^* = (x^* - L/2)\tan\alpha$. In each experiment, the tank was rotated in the anticlockwise direction and so we can relate our coordinates to the standard β-plane convention [17, 21] by referring to the up-slope x-direction as north, and the along-slope y-direction as west (as shown in Fig. 1).

Application of the PIV algorithm produced measurements of $u^*(x^*, y^*, t^*)$ and $v^*(x^*, y^*, t^*)$ in the horizontal plane at $z^* = b$, together with measurements of the

corresponding vertical vorticity component, henceforth denoted ω^*. So that the vertical structure of the flow could be analysed, each experiment was first performed with the light sheet positioned at a height $b = 8\,\text{cm} \approx 0.35H$ or $10\,\text{cm} \approx 0.43H$, and then repeated under near-identical conditions but with the light sheet positioned closer to the slope at $b = 5\,\text{cm} \approx 0.22H$ or $7\,\text{cm} \approx 0.30H$ (respectively). We describe the flow's structure and development using contours of the streamfunction ψ^*, related to the fluid velocity by $(u^*, v^*, 0) = -\nabla \psi^* \times \mathbf{k}$, where $\mathbf{k}$ is the unit vector in the z^*-direction. The streamfunction ψ^* was computed directly from the measured vertical vorticity ω^*, which are related by $\nabla^2 \psi^* = -\omega^*$, with $\psi^* = 0$ at the container sidewalls. The Poisson equation was solved
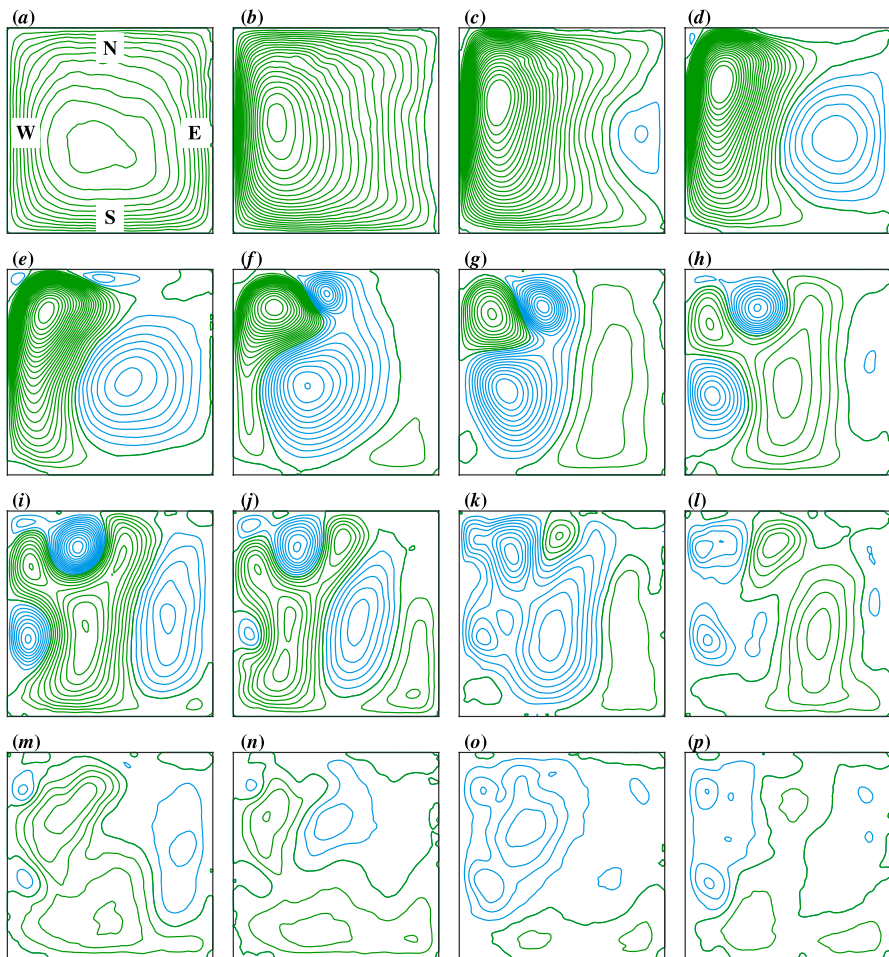
Fig. 2 Measured streamlines from experiment A ($\Omega = 1.1\,\text{rad/s}$, $S = 0$) at the height $z = 0.43h$. The dimensionless times t at which the data were taken are **a** 0, **b**) 8.8, **c** 18, **d** 26, **e** 35, **f** 53, **g** 70, **h** 97, **i** 114, **j** 141, **k** 167, **l** 194, **m** 220, **n** 246, **o** 273, **p** 300. The negative green contours (anticyclonic flow) are uniformly distributed from 0 at increments of -0.16 for $t < 100$ (-0.08 at later times). The positive blue contours (cyclonic flow) are uniformly distributed from 0 at increments of 0.16 for $t < 100$ (0.08 at later times). The top (North) and bottom (South) of the inclined base are shown in (*a*)

using successive line over relaxation. Examples of the computed streamlines are shown in Fig. 2.

Henceforth we shall throughout use the dimensionless variables

$$t \equiv \Omega t^*, \quad \mathbf{x} = (x, y, z) \equiv \frac{\mathbf{x}^*}{L}, \quad \mathbf{u} = (u, v, w) \equiv \frac{\mathbf{u}^*}{\epsilon \Omega L}, \tag{2}$$

which is the same scaling used previously in Munro & Foster [20].

2.3 Observations

2.3.1 Homogeneous fluid ($S = 0$)

Figure 2 shows streamline data for $S = 0$ (experiment A; see Table 1). Shortly after starting the experiment, the observed flow, relative to the rotating reference frame, consists of a central anticyclone with closed streamlines that fill the tank's interior (Fig. 2a). The Ekman layers and sidewall boundary layers are not fully formed at early times and so the interior flow is effectively inviscid and two dimensional. In the sliced cylinder configuration, the vortex lines of the initial flow are stretched when advected down the slope, producing vorticity relative to the rotating reference frame. This results in the formation, on the $\alpha^{-1} \Omega^{-1}$ time scale, of alternating cyclonic and anticyclonic vorticity waves, which originate adjacent to the eastern sidewall and propagate westwards across the slope.

The first vorticity wave, which is cyclonic, is evident in Fig. 2c forming adjacent to the eastern sidewall, as the initial anticyclone moves westwards. To help the reader easily identify the different vorticity waves, the negative streamlines (anticyclonic) are shown in green and the positive streamlines (cyclonic) shown in blue. Fig. 2c–f show the cyclonic first vorticity wave propagating westwards. During this period the initial anticyclone not only moves westwards but also northwards up the slope, eventually accumulating in the north-west corner region of the tank. The intensification of the anticyclonic flow in the north-west corner region results in a local break down of the sidewall boundary layers, and the subsequent formation of two secondary cyclonic vortices: one forms in the vertex of the north-west corner; the other forms adjacent to the north sidewall, which is downstream of the corner relative to the anticyclonic flow. Both of the secondary vortices are clearly evident, shortly after formation, in Fig. 2e. At the subsequent times shown in Fig. 2f and g, we observe a rapid growth of the secondary vortex on the north sidewall, which starts to merge with the westward-moving cyclonic first vorticity wave.

Figure 2g–i show the anticyclonic second vorticity wave forming at the eastern sidewall and moving westwards across the tank. As the second wave approaches the western sidewall, the merging of the cyclonic first wave with the secondary cyclonic vortex is impeded, until they are eventually pinched (see Fig. 2h). This allows the vorticity accumulated in the north-west corner, originally associated with the initial anticyclone, to merge with the anticyclonic second vorticity wave (Fig. 2i).

A similar pattern is observed at subsequent times, with vorticity waves continuing to form adjacent to the eastern side, which propagate westwards and merge with vorticity associated with previous waves. For example, Fig. 2i and j show the cyclonic third vorticity wave propagating westwards, which merges with the vorticity initially associated with the cyclonic first wave and secondary vortices (Fig. 2k). At the later times shown in Fig. 2l and m we see evidence of the fourth (anticyclonic) and fifth (cyclonic) vorticity waves, respectively, although during these later stages the wave amplitudes
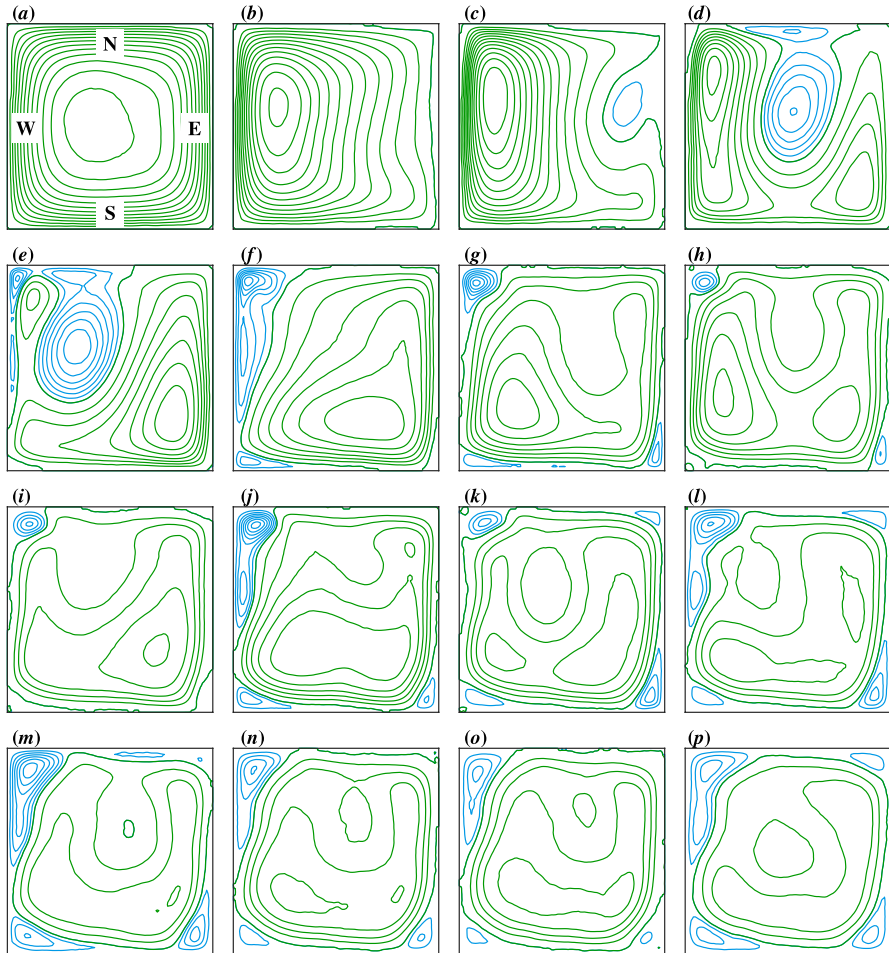
Fig. 3 Measured streamlines from experiment B ($\Omega = 1.04$ rad/s, $S = 0.5$) at the height $z = 0.43h$. The dimensionless times t at which the data were taken are **a** 0, **b** 8.3, **c** 17, **d** 29, **e** 42, **f** 58, **g** 71, **h** 87, **i** 100, **j** 125, **k** 154, **l** 179, **m** 208, **n** 234, **o** 270, **p** 304. The negative green contours (anticyclonic flow) are uniformly distributed from 0 at increments of -0.2 for $t < 100$ (-0.15 at later times). The positive blue contours (cyclonic flow) are uniformly distributed from 0 at increments of 0.08 for $t < 100$ (0.05 at later times). The top (North) and bottom (South) of the inclined base are shown in (a)

are much reduced. Eventually the vorticity waves fill the interior domain and the fluid attains a mostly spun-up state; only a weak residual flow remains (Fig. 2p), which gradually decays

Experiment A was repeated, but instead with the velocity measurements obtained closer to the slope, in the horizontal plane at height $z = 0.30h$. When compared, we found no discernible difference between these data and those shown in Fig. 2 (for $z = 0.43h$), which confirms—as one would expect for homogeneous, small-Rossby-number flow—that the Taylor-Proudman theorem applies and the interior flow is two-dimensional.

2.3.2 Density stratified fluid ($S > 0$)

The introduction of a linear density stratification has a significant affect on the observed flow. This is illustrated by Fig. 3, which shows streamline data from experiment B, for $S = 0.5$ (see Table 1), which corresponds to the case of a relatively weak density gradient. Initially, the flow features are similar to those observed for $S = 0$, with the initial formation of a central anticyclone (Fig. 3a), which subsequently moves westwards and northwards as the cyclonic first vorticity wave forms at the eastern sidewall and moves westwards (Fig. 3b–d). Again, we observe the formation of secondary cyclonic vortices due to the intensified anticyclonic flow in the north-west corner, with the north-wall secondary vortex growing and merging with the cyclonic first wave as it moves westwards (Fig. 3d and e).

However, a number of key differences are clearly evident. Firstly, for $S = 0.5$ there is a weak north-south asymmetry clearly evident in the structure of the vorticity waves. That is, the cyclonic first wave propagates westwards, but does so with its centre located slightly north of the centreline $x = 0.5$ (see Fig 3c–e). Likewise, the subsequent anticyclonic second wave propagate westwards with its centre located south of $x = 0.5$ (Fig. 3e–g). This is in stark contrast to what we observed for $S = 0$, where the westward-moving cyclonic and anticyclonic waves initially propagate along the centreline $x = 0.5$ (see Fig. 2).

Another notable difference evident for $S = 0.5$ is that the wave amplitudes are more rapidly damped compared to the $S = 0$ case. That is, for $S = 0.5$ we observe the cyclonic first and third vorticity waves (*e.g.* see Fig. 3d and h), but there is no discernible visual evidence of cyclonic waves forming at later times. Likewise, we observe the anticyclonic second and fourth waves (*e.g.* see Fig. 3e and i), and although the data suggest the possible formation of anticyclonic waves at subsequent times, they are of small amplitude.

Hence, for $S = 0.5$, the flow domain does not fill with vorticity waves in the same way as described above for $S = 0$. Instead, a quasi steady state develops where the domain is almost entirely filled by a residual anticyclonic flow (see Fig. 3m–p), which results in the formation of secondary cyclonic cells in the vertical corner regions of the container, which are similar to the corner cells that form when fluid is spun-up in a uniform depth square cylinder [14]. The residual anticyclonic flow decays slowly due to the action of the lid and base Ekman layers, and the inwardly growing sidewall boundary layers.

Experiment B was repeated with data obtained closer to the slope at height $z = 0.3h$. Slight differences are evident between these data and those shown in Fig. 3 (for $z = 0.43h$), indicating a z-dependence to the structure of vorticity waves. However, this vertical wave structure is relatively weak for $S = 0.5$. Hence, to better illustrate and describe this structure we now consider the data obtained for increasingly larger values of S, where the z-dependence to the wave structure becomes increasingly more pronounced.

Figure 4 shows data obtained from experiment C, for $S = 1.1$ (see Table 1). In this case the figure is formatted to show data obtained at two different heights, at corresponding times. That is, the two left-hand columns in Fig. 4, labelled (*i*), show data obtained at height $z = 0.22h$; the two right-hand columns, labelled (*ii*), show data obtained further from the slope, at height $z = 0.35h$ (see figure caption for details). Note that, although the data were obtained from separate experiments, the two experiments were performed under essentially identical conditions, and so direct comparisons can be made.

At early times, we again observe the formation of a central anticyclone (see Fig. 4i,a and *ii,a*). Let us now consider the data obtained closest to the slope at height $z = 0.22h$.
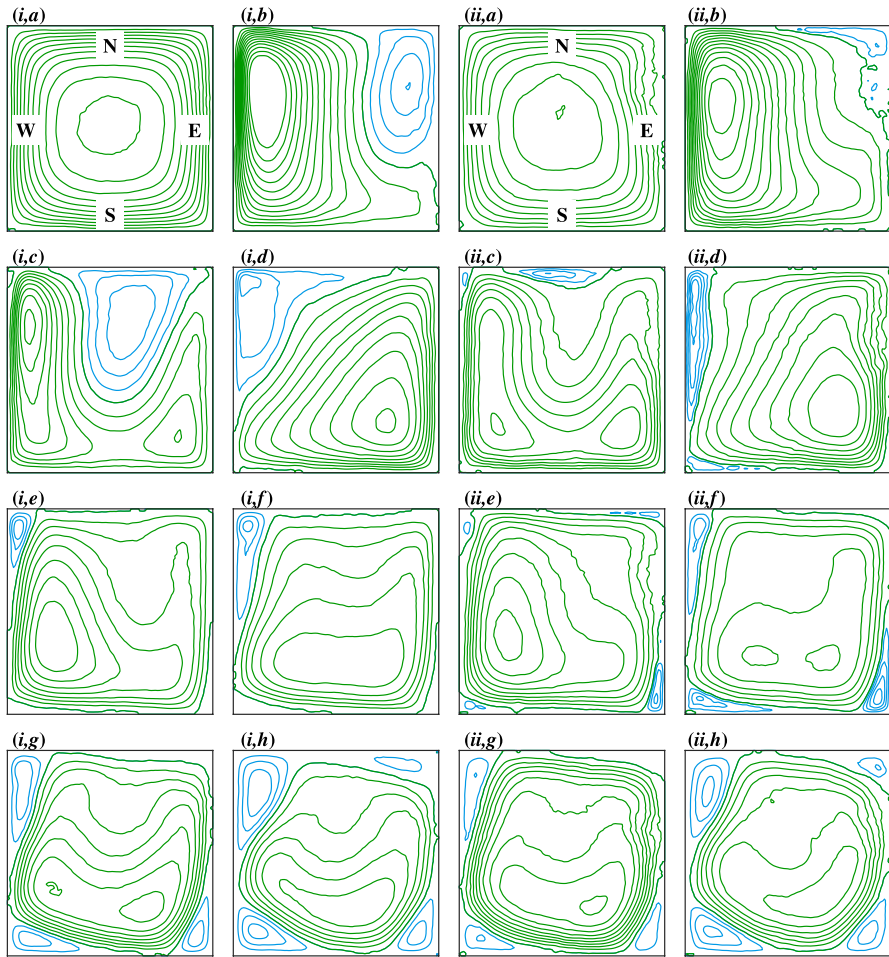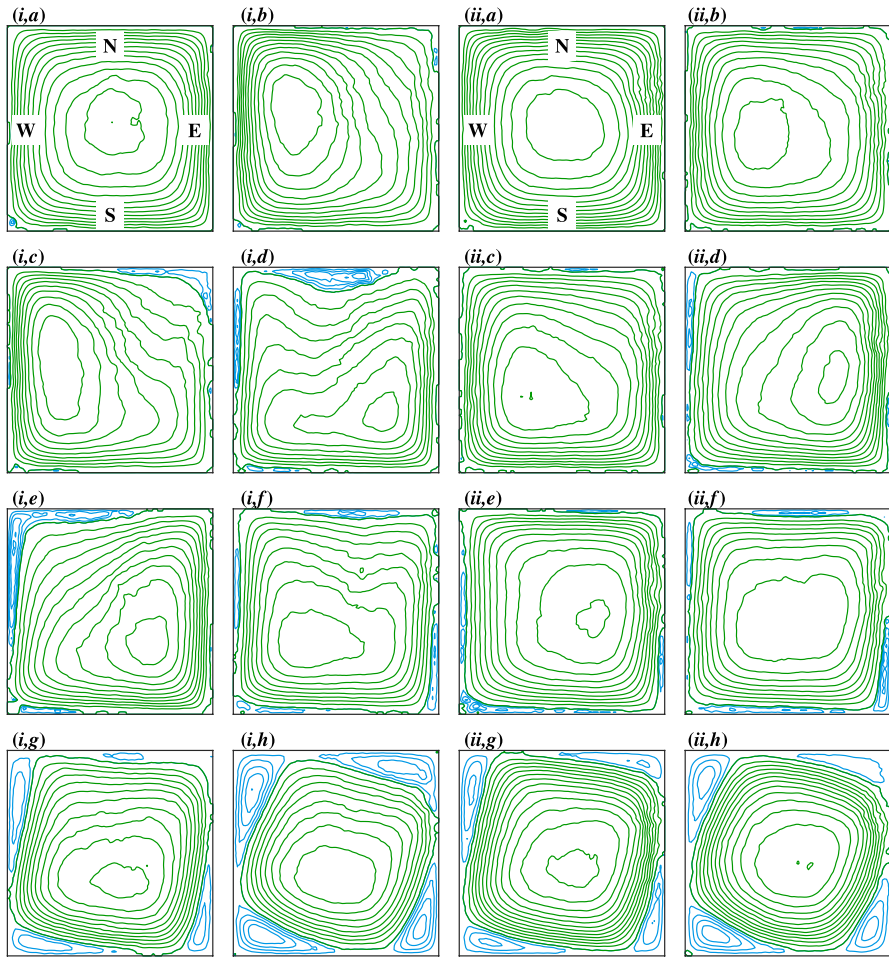
Fig. 4 Measured streamlines from experiment C ($\Omega = 1.04$ rad/s, $S = 1.1$). The data shown in the left-hand columns, denoted (*i*), were obtained at the height $z = 0.22h$. The data in the right-hand columns, denoted (*ii*), were obtained at $z = 0.35h$. The dimensionless times t at which the data were taken are ***a*** 0, ***b*** 12, ***c*** 21, ***d*** 37, ***e*** 54, ***f*** 87, ***g*** 179, ***h*** 320. The negative green contours (anticyclonic flow) are uniformly distributed from 0 at increments of -0.2 for $t < 100$ (-0.12 at later times). The positive blue contours (cyclonic flow) are uniformly distributed from 0 at increments of 0.15 for $t < 100$ (0.1 at later times). The top (North) and bottom (South) of the inclined base are shown in (*a*)

In Fig. 4(*i*,*b*–*d*) the cyclonic first vorticity wave is clearly visible, forming adjacent to the eastern sidewall and propagating westwards, subsequently followed by the anticyclonic second vorticity wave (Fig. 4*i*,*c*–*e*). The distinct north-south asymmetry in the alternating wave structure is again clearly evident. However, what is notable at this slightly larger value of *S*, compared to the data shown in Fig. 3 for $S = 0.5$, is that the waves are more severely damped, with no discernible evidence in the data of any further vorticity waves forming—if they do form, they are certainly of small amplitude. At subsequent times, we again observe the formation of cyclonic corner cells as the residual anticyclonic flow gradually decays (Fig. 4*i*,f–h).

Comparing these data at corresponding times with the data obtained at height $z = 0.35h$, shown in Fig. 4(ii), we observe a distinct vertical structure evident in the vorticity waves for $S = 1.1$—in particular, in the structure of the cyclonic first wave. That is, the cyclonic first wave is evident in Fig. 4(ii,b–d), as it propagates westwards. However, further from the slope, at height $z = 0.35h$, the cyclonic wave structure is confined further northwards in a narrow region close to the northern sidewall, as it moves westwards. Hence, it appears that increasing S results in the vorticity waves becoming increasingly confined to a region above the base slope, and the further above the mean slope elevation, that region is increasingly confined closer to the northern wall. Hence, for some height $z > 0.35h$, for $S = 1.1$,
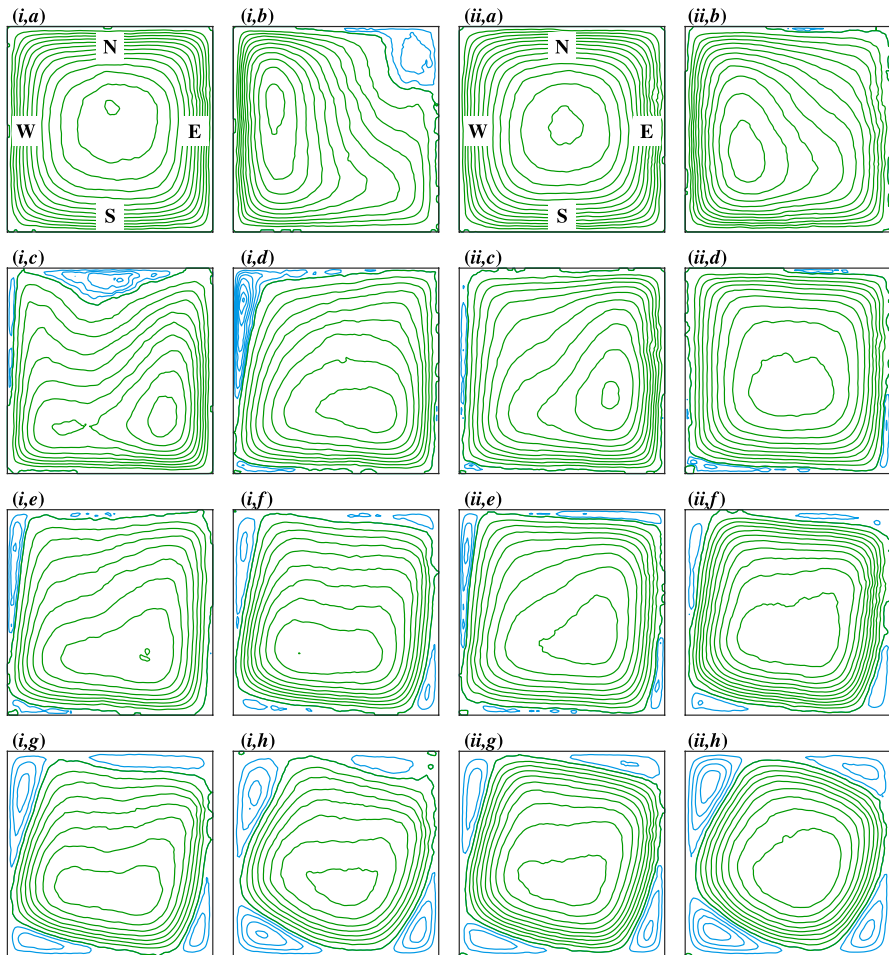
Fig. 5 Measured streamlines from experiment D ($\Omega = 0.48$ rad/s, $S = 5.0$). The data shown in the left-hand columns, denoted (i), were obtained at the height $z = 0.22h$. The data in the right-hand columns, denoted (ii), were obtained at $z = 0.35h$. The dimensionless times t at which the data were taken are $\boldsymbol{a}$ 0, $\boldsymbol{b}$ 5.8, $\boldsymbol{c}$ 14, $\boldsymbol{d}$ 21, $\boldsymbol{e}$ 37, $\boldsymbol{f}$ 60, $\boldsymbol{g}$ 83, $\boldsymbol{h}$ 149. The negative green contours (anticyclonic flow) are uniformly distributed from 0 at increments of -0.2 for $t < 100$ (-0.15 at later times). The positive blue contours (cyclonic flow) are uniformly distributed from 0 at increments of 0.05 for $t < 100$ (0.08 at later times). The top (North) and bottom (South) of the inclined base are shown in (a)

Fig. 6 Measured streamlines from experiment E ($\Omega = 0.34$ rad/s, $S = 10$). The data shown in the left-hand columns, denoted (*i*), were obtained at the height $z = 0.22h$. The data in the right-hand columns, denoted (*ii*), were obtained at $z = 0.35h$. The dimensionless times t at which the data were taken are *a* 0, *b* 2.7, *c* 4.1, *d* 9.6, *e* 12, *f* 21, *g* 55, *h* 96. The negative green contours (anticyclonic flow) are uniformly distributed from 0 at increments of -0.2 for $t < 100$ (-0.15 at later times). The positive blue contours (cyclonic flow) are uniformly distributed from 0 at increments of 0.04 The top (North) and bottom (South) of the inclined base are shown in (*a*)
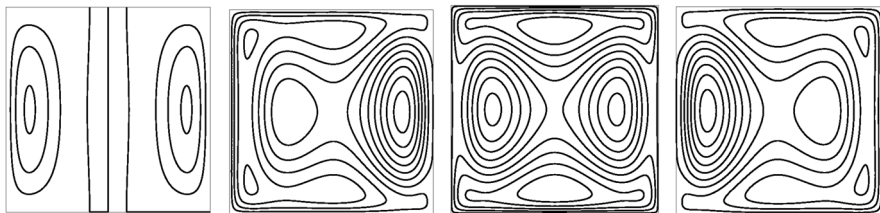
Fig. 7 Computed Rossby-wave mode shape for $S = 0.5$, $\lambda = 0.706$; $\alpha\lambda\Omega$ is the circular frequency of this mode. Instantaneous streamlines sequence for $\lambda\tau = 0, \pi/4, \pi/2, 3\pi/4$ (from left to right)

the vorticity waves would not be present in horizontal-plane streamline pattern. This latter point is better illustrated by the data shown in Figs. 5 and 6, which are for $S = 5$ and 10 respectively. These data show that the cyclonic first wave is evident at height $z = 0.22h$, and becomes confined closer the northern sidewall with increasing S (*e.g.* compare Figs. 5*i,b–d* and 6*i,b-d*). However, further above the slope at height $z = 0.35h$, there is no visible evidence of the cyclonic first wave at these times (*e.g.* Figs. 5*ii,b–d* and 6*ii,b–d*). The analysis presented in Munro & Foster [21], for a circular sliced cylinder, showed that the vorticity waves are trapped within an increasingly shallower region of height $S^{-1/2}$ above the mean slope elevation. In general, the data presented here are in agreement with this result, where, for example, the vorticity waves are evident in the data at height $z = 0.35h$ for $S \gtrsim 5$. For convenience, the corresponding values of $S^{-1/2}$ for each experiment are shown in Table 1.

Finally, we note that the data in Figs. 3, 4, 5, 6 also suggest there is S-dependency in the propagation speed of the vorticity waves; that is, the wave speed increases with increasing S. For example, estimates of the scaled time t for the cyclonic first wave to traverse the slope are $\approx$ 40, 30, 15 and 10, for $S = 0.5, 1.1, 5$ and 10, respectively. (Note, it is difficult to estimate the corresponding traverse time for $S = 0$, as the wave's trajectory is significantly affected by the merging events; and for $S = 20$ the vorticity waves are trapped in a region below $z = 0.22h$ and so were not visible in our $S = 20$ data.)

3 Some comments on the theory

A complete theoretical treatment of the small-Rossby number spin up is contained in Munro & Foster [20], and that will not be repeated here, apart from a brief summary of some of the principal results. With time, lengths and velocities scaled as shown in equation (2), the vertical walls are located at $x = 0, 1$ and $y = 0, 1$—denoted here by $\mathscr{D}_v$. The lower boundary is at $z = \alpha(x - 1/2)$, and the upper boundary is located at $z = h$. The scaled Cartesian velocity components, (u, v, w), can be written

$$u = -\frac{1}{2}p_y, \quad v = \frac{1}{2}p_x, \quad w = -\frac{1}{S}p_{zt}, \tag{3}$$

and, quoting from [20], the dimensionless modified pressure p, which as been scaled by $\epsilon \rho_t \Omega^2 L^2$, obeys the equation

$$\mathscr{L}\{p\} = \nabla_1^2 p + \frac{4}{S}p_{zz} = -4 \text{ in } \mathscr{V}, \tag{4}$$

where ∇_1^2 is the horizontal Laplacian. In that cited paper, Ekman suction terms are included, and provide the damping for the Rossby waves. Those terms are not shown here for the sake of simplicity in the discussion; those terms do not affect the arguments below. Here, $\mathscr{V}$ denotes the interior of the container. The impermeability condition gives $p = 0$ on $\mathscr{D}_v$, and on the upper and lower boundaries,

$$p_z = 0 \text{ on } z = h, \tag{5}$$

$$\mathscr{M}\{p\} = p_{zt} - \frac{1}{2}Sp_y = 0 \text{ on } z = \alpha\left(x - 1/2\right), \tag{6}$$

where the time has been scaled with the slope, so

$$\tau \equiv \alpha t. \tag{7}$$

Of the number of small parameters in the experiments reported here, α is much bigger than either ϵ or $E^{1/2}$, so the asymptotic series begins

$$p = p_1 + \alpha p_2 + \dots. \tag{8}$$

Then, p_1 satisfies

$$\mathscr{L}\{p_1\} = -4 \text{ in } \mathscr{V}, \quad p_{1z} = 0 \text{ on } z = h, \quad \mathscr{M}\{p_1\} = 0 \text{ on } z = 0, \tag{9}$$

since the lower boundary condition has been "transferred" to $z = 0$. The initial-value problem is discussed in [20], by seeking solutions to the associated spatial eigenvalue problem. In that paper, we report that the circular frequencies lie between 0 and $\sqrt{S}$, where we have also found that the damping due to the Ekman layers on top and bottom of the container does not occur on the usual "spin-up" time, $E^{-1/2}$, but rather on the (smaller) time scale $E^{-1/2}/\log(E^{1/2}/\alpha)$. We also have found that the Rossby waves with frequency closer to $\sqrt{S}$ damp more rapidly than those at smaller frequencies.

Instantaneous streamlines for a particular time-periodic Rossby mode are shown in Fig. 7, for $S = 0.5$, for one oscillation period. The westward propagation is evident. One notes the similarity to some of members of Fig. 3, from the experiments. However, what is also immediately apparent is that the distinct north-south asymmetry evident in the experimental results stands in stark constant with the north-south symmetry in the theoretical results. From equation (9), it is clear that replacing $x - 1/2$ by $1/2 - x$ changes nothing, hence the north-south symmetry in the theory is easy to see.

However, working to the next order in the asymptotic series,

$$\mathscr{L}\{p_2\} = 0 \text{ in } \mathscr{V}, \tag{10}$$

and

$$p_{2z} = 0 \text{ on } z = h, \quad \mathscr{M}\{p_2\} = -\frac{S}{4}(x - 1/2)\left[\nabla_1^2 p_{1,\tau} + 2p_{1,zy}\right] \text{ on } z = 0. \tag{11}$$

In this case, replacing $x - 1/2$ by $1/2 - x$ leaves the square bracket unchanged in equation (11), but the $(x - 1/2)$ multiplier means that, in fact, p_2 is NOT north-south symmetric. So we conclude that α is sufficiently large to make a one-term solution not particularly reliable in terms of Rossby-wave mode shapes. Modifying the results given in [20] to include the α term in the series is beyond the scope of this paper and will be reported elsewhere.

4 Final remarks

Our results show the westward propagation of Rossby waves as the mechanism for the spin up in sliced square cylinder, when S is small. As S is increased much beyond 1, the Rossby waves become increasingly trapped in a layer above the mean slope elevation, of height that scales with $S^{-1/2}$. So, for large S, the bulk interior flow above the trapped layer is largely unaffected by the Rossby waves, and takes the form of a gradually decaying central anticyclone, with cyclonic vortices forming in the vertical corner regions. Of course, there also exists a layer of thickness $S^{-1/2}$ below the tank's lid; the role of this layer is to receive the fluid erupting from the perimeter region of the lid Ekman layer [5]. Hence, for large S,

the interior flow is similar to what we observe for the case of a spin-up in a uniform depth square cylinder [14], with the spin-up achieved by Ekman pumping and the inward growth of the sidewall boundary layers.

There are a number of additional conclusions to be drawn, noted below.

1. The flow patterns evidenced in Figs. 2 to 6 show that the small-scale waves for $S = 0$ and also for $S = 0.5$ give way to waves with much larger scales at larger values of S.
2. The time scales are instructive. The characteristic time for Rossby-wave propagation is $t \sim \alpha^{-1} = 5.7$. As we have noted, the Rossby-wave damping by Ekman pumping is $t \sim E^{-1/2} / \log(\alpha / E^{1/2}) = 52$. It is noteworthy that the boundary-layer eruption time scale is precisely the same order, namely $t \sim Ro^{-1} = 50$. By comparing Fig. 3 and Fig. 7, it is clear that the vortices in Fig. 3(*a–d*) are, in fact, in the Rossby-wave structure, and NOT due to boundary-layer eruption. In fact, the vortices first appearing at north-west and south-east corners in Fig. 3(*f–i*), remain remarkably confined to the corners to quite long times.
3. The simple, leading-order theory, from which we have determined Rossby-wave frequencies, in [20], does not compare well with our experimental results because the slope is too large to make the theory adequate, as we have shown. A second-order correction is required in order to exhibit the north-south asymmetry so much in evidence in the experiments.

This paper is presented in honor of the body of work in environmental fluid mechanics by Professer P.A. Davies. We are grateful for his amazing insights into fluid motions and his generosity to his collaborators, but most of all we appreciate his friendship. Thanks Pete!

Declarations

References

1. Greenspan HP, Howard LN (1963) On a time-dependent motion of a rotating fluid. J Fluid Mech 17:385
2. Greenspan HP (1965) On the general theory of contained rotating fluid motions. J Fluid Mech 22:449
3. Wedemeyer EH (1964) The unsteady flow within a spinning cylinder. J Fluid Mech 20:383
4. Holton JR (1965) The influence of viscous boundary layers on transient motions in a stratified rotating fluid. Part I. J Atmos Sci 22:402
5. Walin G (1969) Some aspects of time-dependent motion of a stratified rotating fluid. J Fluid Mech 36(2):289

6. Sakurai T (1969) Spin down problem of rotating stratified fluid in thermally insulated circular cylinders. J Fluid Mech 37(4):689
7. Stewartson K (1957) On almost rigid rotations. J Fluid Mech 3:17
8. Benton ER, Clark A (1974) Spin-up. Annu Rev Fluid Mech 6:257
9. Duck PW, Foster MR (2001) Spin-up of homogeneous and stratified fluids. Annu Rev Fluid Mech 33:231
10. van Heijst GJF (1989) Spin-up phenomena in non-axisymmetric containers. J Fluid Mech 206:171
11. van Heijst GJF, Davies PA, Davis RG (1990) Spin-up in a rectangular container. Phys Fluids A 2:150
12. van Heijst GJF, Maas LRM, Williams CWM (1994) The spin-up of fluid in a rectangular container with a sloping bottom. J Fluid Mech 265:125
13. van de Konijnenberg JA, van Heijst GJF (1997) Free-surface effects on spin-up in a rectangular tank. J Fluid Mech 334:189
14. Foster MR, Munro RJ (2012) The linear spin-up of a stratified, rotating fluid in a square cylinder. J Fluid Mech 712:7
15. Munro RJ, Hewitt RE, Foster MR (2015) On the formation of axial corner vortices during spin-up in a cylinder of square cross section. J Fluid Mech 772:246
16. Munro RJ, Foster MR (2022) Spin-up in a semicircular cylinder. J Fluid Mech 938:A15
17. Pedlosky J, Greenspan HP (1967) A simple laboratory model for the oceanic circulation. J Fluid Mech 27:291
18. Beardsley RC (1969) A laboratory model of the wind-driven ocean circulation. J Fluid Mech 38(2):255
19. Beardsley RC, Robbins K (1975) The 'sliced cylinder' laboratory model of the wind-driven ocean circulation. Part 1. Steady forcing and topographic Rossby wave instability. J Fluid Mech 69(1):27
20. Munro RJ, Foster MR (2014) Stratified spin-up in a sliced, square cylinder. Phys Fluids 26:026603
21. Munro RJ, Foster MR (2016) The spin-up of a linearly stratified fluid in a sliced, circular cylinder. J Fluid Mech 806:254
22. Greenspan HP (1968) The Theory of Rotating Fluids. Cambridge University Press
23. Economidou M, Hunt GR (2009) Density stratified environments: the double-tank method. Exp Fluids 46:453
24. Munro RJ, Foster MR, Davies PA (2010) Instabilities in the spin-up of a rotating, stratified fluid. Phys Fluids 22:054108